Chen *et al.*
Natural Products and Bioprospecting (2026) 16:4
https://doi.org/10.1007/s13659-025-00557-0

Natural Products and Bioprospecting

ORIGINAL ARTICLE

Open Access

Diverse phloroglucinols with *h*AChE inhibitory and anti-VRE effects from *Rhodomyrtus tomentosa* fruits

Ling-Yun Chen[1,2†], Mu-Yuan Yu[2†], E-E Luo[2,3†], Wen-Ying Zong[2,3], Shu-Mei Lei[2,3], Yu Pan[2,3], Ai-Chun Lu[2,3], Cheng-Qin Liang[1*] and Xu-Jie Qin[2,3*]

Abstract

Rhodomyrtus tomentosa fruits serve as both functional food and medicinal resources due to their rich bioactive constituents and manifold pharmacological effects. Phytochemical exploration of the *R. tomentosa* fruits led to the identification of eight new polymethylated phloroglucinols, designated as rhodotomentodione F (**1**) and rhodotomentodimers H–N (**2–8**), along with six previously described congeners (**9–14**). Based on the detailed inspection of comprehensive spectroscopic data, electronic circular dichroism (ECD) simulations, and nuclear magnetic resonance (NMR) calculations, and DP4+ analyses, the structures of phloroglucinols **1–8** were determined. Heterodimeric phloroglucinols **3–14** exhibited human acetylcholinesterase (*h*AChE) inhibitory activities, with **13** exhibiting the highest potency (IC_{50} = 1.04 μM). Moreover, molecular docking analysis clarified the potential binding interactions between the most active phloroglucinol **13** with *h*AChE. In addition, phloroglucinols **11** and **12** displayed significant anti-VRE (vancomycin-resistant *Enterococci*) activities, with MIC values reaching as low as 1 μg/mL.

Keywords *Rhodomyrtus tomentosa* fruits, Phloroglucinols, *h*AChE inhibitory activity, Anti-VRE activity, Molecular docking

†Ling-Yun Chen, Mu-Yuan Yu and E.-E. Luo contributed equally.

*Correspondence:
Cheng-Qin Liang
cqliang@glmc.edu.cn
Xu-Jie Qin
qinxujie@mail.kib.ac.cn
Full list of author information is available at the end of the article

Graphical Abstract

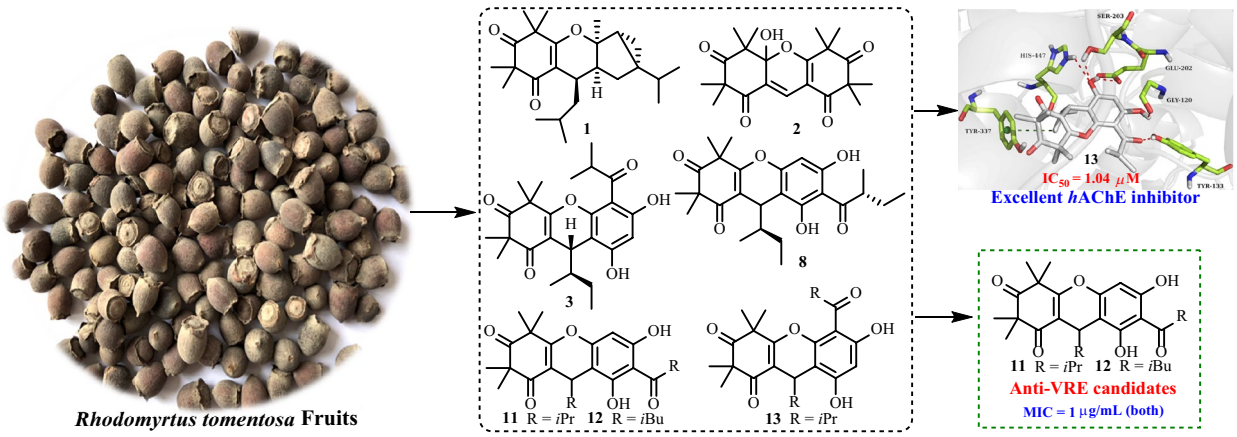

1 Introduction

Phloroglucinols derived from species within the Myrtaceae family have garnered significant attention from scientific community due to their complex molecular architectures and notable biological activities [1]. *Rhodomyrtus tomentosa*, a medicinal and edible plant of this family, is extensively cultivated across Thailand, Vietnam, and southeastern China [2]. The *R. tomentosa* fruits are popularly used as ingredients of pies and jams in these regions [3]. Furthermore, local populations traditionally infuse the fruits into white spirits to prepare herbal liquors, which are valued for their enhanced flavor and health-promoting and disease-preventive properties. Historically, the fruits, have also been utilized for the management of diarrhea and dysentery [3]. Previous studies have demonstrated that crude extracts and phenolic constituents from *R. tomentosa* fruits exhibit antioxidant [4–6], anti-inflammatory [7, 8], hepatoprotective effects against nonalcoholic fatty liver disease [9], and general health-promoting benefits [10]. Despite these findings, only one phloroglucinol homodimer with anti-inflammatory activity, namely watsonianone A [11], has been identified from the fruits of title plant, leaving the broader phloroglucinol composition largely unexplored. In contrast, phloroglucinol compounds isolated from *R. tomentosa* leaves in tropical regions of China have been characterized for both structures and their bioactivities [12–16]. Therefore, further elucidation of novel bioactive phloroglucinol components from its fruits represents a valuable research direction. To obtain additional active phloroglucinol constituents, the fruits were subjected to ultraviolet-guided employing a DAD detector. Consequently, eight newly reported polymethylated phloroglucinols (**1**–**8**) and six known analogues (**9**–**14**) were obtained (Fig. 1). Selected compounds were examined for their *h*AChE inhibitory and anti-VRE activities. For the most potent *h*AChE inhibitor, molecular docking analysis was conducted to elucidate the possible interaction mechanism. This study presents the isolation, comprehensive structural characterization, and preliminary pharmacological assessment of the isolated metabolites.

2 Results and discussion

The phloroglucinol containing moiety of *R. tomentosa* fruits was subjected to sequential chromatographic separation on silica gel, reversed-phase C18, Sephadex LH-20, and semi-preparative HPLC, leading to the isolation of one new polymethylated phloroglucinol meroterpenoid (PPM, **1**), one new polymethylated phloroglucinol homodimer (PPHMD, **2**), and six polymethylated phloroglucinol heterodimers (PPHTDs, **3**–**8**). In addition, six previously reported congeners were structurally identified as myrciarone B (**9**) [17, 18], rhodotomentodimer D (**10**) [13], isomyrtucommulone B (**11**) [17, 18], rhodomyrtone (**12**) [19], myrtucommulone B (**13**) [20], and callistenone A (**14**) [21], based on detailed comparison of their NMR and mass spectrometry (MS) profiles with reference data previously documented in the literature.

Phloroglucinol **1** was assigned the molecular formula of $C_{25}H_{38}O_3$, as determined by an high-resolution electrospray ionization mass spectrometry (HRESIMS) with an $[M+H]^+$ ion at m/z 387.2904 (calcd for $C_{25}H_{39}O_3$, 387.2894), indicating seven degrees of unsaturation. The ^{1}H NMR spectrum (Table 1) displayed signals for nine methyl groups at δ_H 0.85 (d, J=6.8 Hz, H_3-10′), 0.86 (d, J=6.8 Hz, H_3-9′), 0.89 (d, J=6.6 Hz, H_3-11), 0.95 (d, J=6.6 Hz, H_3-10), 1.33 (s, H_3-13), 1.34 (s, H_3-12), 1.38 (s, H_3-15), 1.40 (s, H_3-14), and 1.42 (s, H_3-7′), along with

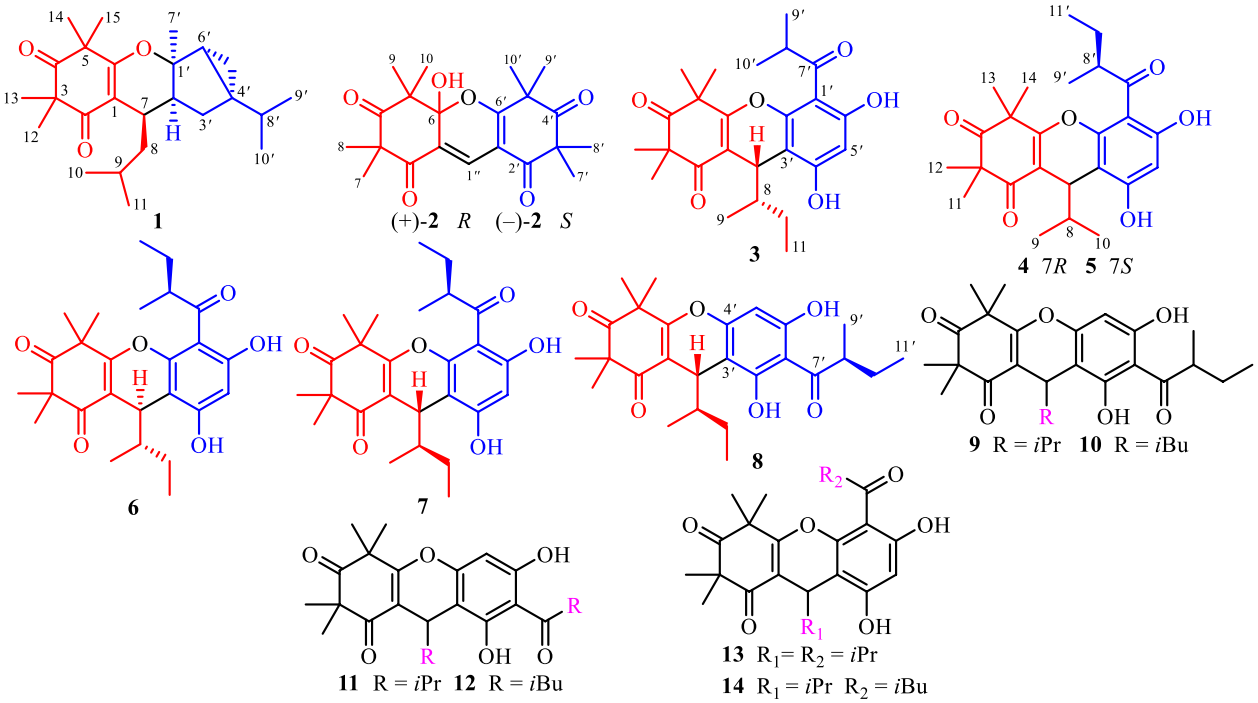

Fig. 1 Chemical structures of phloroglucinols **1**–**14**

two strongly shielded methylene protons at δ_H 0.51 (2H, brd, J=5.4 Hz, H_2-5′), characteristic of a cyclopropane moiety. Analysis of the ^{13}C NMR data of phloroglucinol **1** (Table 1), supported by DEPT and HSQC experiments, disclosed the presence of 25 distinct carbon signals, including two keto carbonyl groups at δ_C 198.3 (C-2) and 213.6 (C-4), two olefinic quaternary carbons at δ_C 109.2 (C-1) and 168.8 (C-6), and additional four quaternary carbons, one of which was oxygenated at δ_C 87.3 (C-1′). The remaining signals were attributed to five methines, three methylenes, and nine methyl groups. Three of the seven degrees of unsaturation were attributed to the presence of two ketone functionalities and a single olefinic bond, while the remaining unsaturation implied the existence of a tetracyclic core structure. The planar architecture of phloroglucinol **1** was determined through comprehensive analyses of ^1H–^1H COSY and HMBC spectra (Fig. 2). The ^1H–^1H COSY experiment established an isopentyl unit of δ_H 2.64 (H-7)/1.29 (H_2-8a) and 1.23 (H_2-8b)/1.67 (H-9)/0.95 (H_3-10) and 0.89 (H_3-11). Key HMBC interactions, from δ_H 2.64 (H-7) to δ_C 109.2 (C-1), 168.8 (C-6), and 198.3 (C-2); from δ_H 1.34 (H_3-12) and 1.33 (H_3-13) to δ_C 55.5 (C-3), 98.3 (C-2) and 213.6 (C-4); and from δ_H 1.40 (H_3-14) and 1.38 (H_3-15) to δ_C 47.7 (C-5), 168.8 (C-6), and 213.6 (C-4), strongly supported the presence of a β-triketone core. Likewise, apart from three structural fragments of δ_H 1.85 (H-2′)/1.34 and 1.74 (H_2-3′), 0.51 (2H, H_2-5′)/1.36 (H-6′), and 1.29 (H-8′)/0.85 (H_3-9′) and 0.86 (H_3-10′) as indicated by the ^1H–^1H COSY spectrum, HMBC correlations (Fig. 2), specifically from δ_H 1.74 (H-3′a) to δ_C 14.2 (C-5′) and 32.4 (C-4′), from δ_H 1.42 (H_3-7′) to δ_C 34.9 (C-6′), 37.6 (C-2′), and 87.3 (C-1′), and

Table 1 ^{13}C (150 MHz) and ^1H (600 MHz) NMR data of phloroglucinol **1** in $CDCl_3$

β-triketone moiety			*α*-thujene unit		
No	δ_C	δ_H, mult. (J in Hz)	No	δ_C	δ_H, mult. (J in Hz)
1	109.2, s		1′	87.3, s	
2	198.3, s		2′	37.6, d	1.85, dd (11.1, 7.5)
3	55.5, s		3′	34.0, t	a 1.74, dd (12.3, 7.5)
4	213.6, s				b 1.34, overlapped
5	47.7, s		4′	32.4, s	
6	168.8, s		5′	14.2, t	0.51, 2H brd (5.4)
7	28.7, d	2.64, dd (10.7, 3.9)	6′	34.9, d	1.36, brd (7.0)
8	42.6, t	a 1.29, m	7′	23.7, q	1.42, s
		b 1.23, m	8′	32.3, d	1.29, overlapped
9	25.7, d	1.67, m	9′	19.6, q	0.86, d (6.8)
10	21.1, q	0.95, d (6.6)	10′	20.0, q	0.85, d (6.8)
11	23.7, q	0.89, d (6.6)			
12	23.2, q	1.34, s			
13	25.7, q	1.33, s			
14	25.1, q	1.40, s			
15	25.2, q	1.38, s			

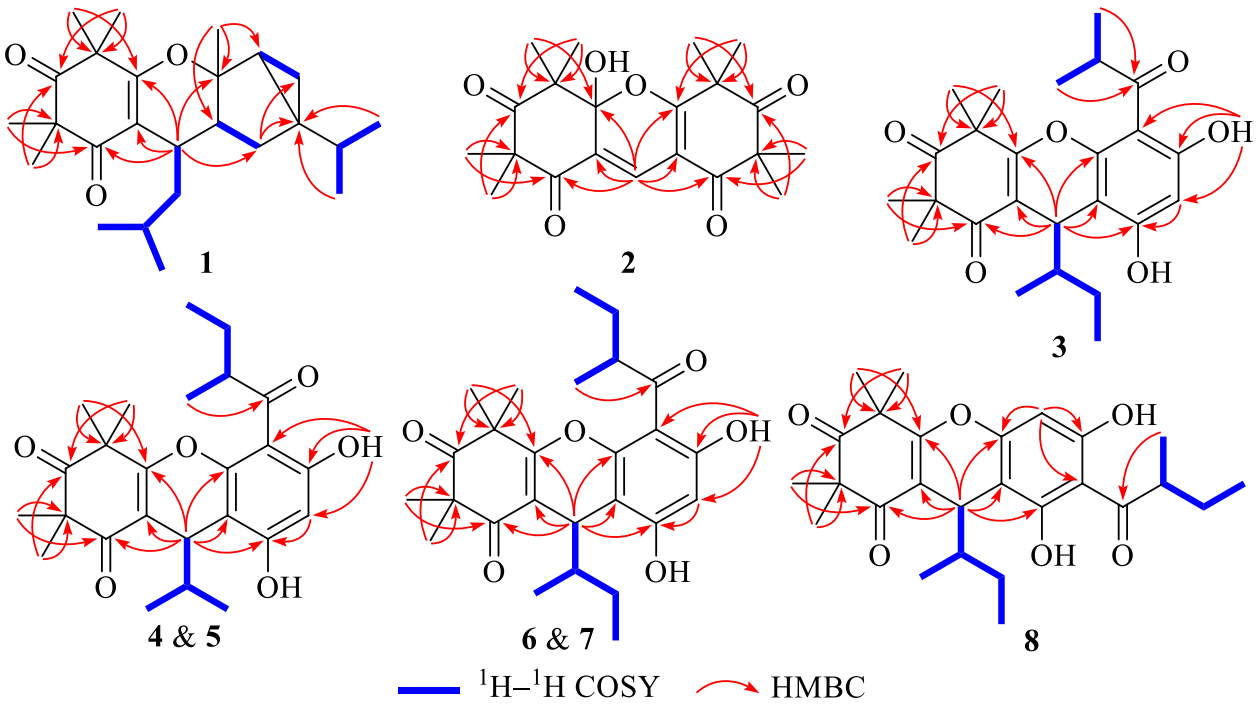

Fig. 2 Key ^{1}H–^{1}H COSY, and HMBC correlations of phloroglucinols **1–8**

from δ_H 0.86 (H_3-9′) and 0.85 (H_3-10′) to δ_C 32.4 (C-4′) confirmed the presence of a thujene unit. Additional HMBC cross-peaks from δ_H 2.64 (H-7) to δ_C 34.0 (C-3′) and 87.3 (C-1′) indicated that the *β*-triketone moiety and the thujene fragment was connected through a C-6–*O*–C-1′ ether linkage and a C-7–C-2′ bond. ROSEY correlations between δ_H 1.85 (H-2′) and 0.51 (H-5′), 1.42 (H_3-7′), and 2.64 (H-7) supported an *α* orientation of all these protons. The assignment of absolute configuration for phloroglucinol **1** was achieved by comparing its measured ECD spectrum with that simulated by TDDFT B3LYP/6–31++G(2d,p) using Gaussian 16. The experimental curve (Fig. 4) exhibited negative Cotton effects at 205 and 271 nm and a positive signal at 311 nm, closely matching the calculated spectrum, thereby confirming the (7*R*,1′*R*,2′*S*,4′*R*,6′*R*) configuration. Based on combined spectroscopic and computational evidence, phloroglucinol **1**, was structurally identified as a novel *β*-triketone–thujene meroterpenoid and designated rhodotomentodione F.

Phloroglucinol **2** was determined to possess the molecular formula $C_{21}H_{26}O_6$, as indicated by HRESIMS, which displayed a $[M+H]^+$ ion at *m*/*z* 375.1802 (cacld for $C_{21}H_{27}O_6$, 375.1802). The ^{1}H NMR spectrum of phloroglucinol **2** (Table 2) featured a downfield singlet at δ_H 8.00 (1H, s, H-1″) and eight singlet methyl groups at δ_H 1.08 (H_3-9), 1.38 (H_3-8), 1.40×2 (6H, H_3-7′/H_3-8′), 1.41 (H_3-7), 1.50 (H_3-10), and 1.53×2 (6H, H_3-9′/H_3-10′). The ^{13}C NMR data revealed four ketone carbonyl signals at δ_C 194.9 (C-2′), 197.1 (C-2), 210.5 (C-4′), and 210.7 (C-4), two double bonds at δ_C 108.3 (C-1′), 122.1 (C-1), 127.7 (C-1″), and 172.9 (C-6′), a hemiketal carbon at δ_C 100.8 (C-6), four quaternary carbons at δ_C 48.0 (C-5′), 53.9 (C-5), 54.8 (C-3), and 56.1 (C-3′), and eight methyl groups, indicating a tricyclic scaffold. Key HMBC correlations (Fig. 2) from δ_H 1.41 (H_3-7) and 1.38 (H_3-8) to δ_C 54.8 (C-3), 197.1 (C-2), and 210.7 (C-4), from δ_H 1.50 (H_3-10) and 1.08 (H_3-9) to δ_C 53.9 (C-5), 100.8 (C-6), and 210.7 (C-4), and from δ_H 8.00 (H-1″) to δ_C 100.8 (C-6),

Table 2 The ^{13}C (150 MHz) and ^{1}H (600 MHz) NMR data of phloroglucinol **2** in $CDCl_3$

No	δ_C	δ_H, mult. (*J* in Hz)	No	δ_C	δ_H, mult. (*J* in Hz)
1	122.1, s		1′	108.3, s	
2	197.1, s		2′	194.9, s	
3	54.8, s		3′	56.1, s	
4	210.7, s		4′	210.5, s	
5	53.9, s		5′	48.0, s	
6	100.8, s		6′	172.9, s	
7	24.2, q	1.41, s	7′	22.9, q	1.40, s
8	26.7, q	1.38, s	8′	23.4, q	1.40, s
9	23.4, q	1.08, s	9′	24.1, q	1.53, s
10	14.9, q	1.50, s	10′	25.4, q	1.53, s
			1″	127.7, d	8.00, s

122.1 (C-1), and 197.1 (C-2) supported a *β*-triketone motif incorporating a hemiketal at C-6 and a C-1 and C-1″ double bond. Similarly, HMBC cross-peaks from δ_H 1.40 (6H, H_3-7′ and H_3-8′) to δ_C 56.1 (C-3′), 194.9 (C-2′), and 210.5 (C-4′), from δ_H 1.53 (6H, H_3-9′/ H_3-10′) to δ_C 48.0 (C-5′), 172.9 (C-6′), and 210.5 (C-4′), and from δ_H 8.00 (H-1″) to δ_C 108.3 (C-1′), 172.9 (C-6′), and 194.9 (C-2′) indicated a second *β*-triketone fragment. Additional HMBC data indicated linkage of the two fragments via a C-6–*O*–C-6′ ether bond and a C-1–C-1″–C-1′ connection. Phloroglucinol **2**, identified as a racemic mixture, was resolved into enantiomers (+)-**2** and (−)-**2** using a Daicel CHIRALPAK IC column. ECD spectral analysis (Fig. 4) established the absolute configurations for (+)-**2** and (−)-**2** to be (6*R*) and (6*S*), respectively. Thus, phloroglucinol **2** was structurally characterized as a PPHMD and designated rhodotomentodimer H.

Phloroglucinol **3** was determined to possess the molecular formula $C_{25}H_{32}O_6$, as established by its HRESIMS, which exhibited a $[M+H]^+$ ion at *m*/*z* 429.2279 (calcd for $C_{25}H_{33}O_6$, 429.2272). The ^{1}H NMR spectrum of phloroglucinol **3** (Table 3) indicated four singlet methyl groups at δ_H 1.39 (H_3-12), 1.42 (H_3-14), 1.43 (H_3-13), and 1.61 (H_3-15), three doublet methyl groups at δ_H 0.74 (*J*=6.8 Hz, H_3-9), 1.24 (*J*=7.3 Hz, H_3-10′), and 1.25 (*J*=6.7 Hz, H_3-9′), a triplet methyl group at δ_H 0.90 (*J*=7.3 Hz, H_3-11). An aromatic proton at δ_H 6.26 (s, H-5′), and a strongly deshielded hydroxyl proton at δ_H 13.30 (s, OH-6′) were also observed. The ^{13}C NMR spectrum (Table 3) displayed 25 carbon resonances, including eight methyl groups at δ_C 12.3 (CH_3-11), 14.9 (CH_3-9), 17.7 (CH_3-9′), 20.8 (CH_3-10′), 24.3 (CH_3-12), 24.5 (CH_3-13), 24.9 (CH_3-14) and 25.1 (CH_3-15), one methylene group at δ_C 26.1 (CH_2-10), three methine groups at δ_C 30.9 (CH-7), 39.7 (CH-8′), and 42.1 (CH-8), two aliphatic quaternary carbons at δ_C 47.2 (C-5) and 56.2 (C-3), a pair of olefinic carbons at δ_C 112.7 (C-1) and 167.5 (C-6), six aromatic carbons at δ_C 100.6 (CH-5′), 103.0 (C-3′), 104.0 (C-1′), 153.8 (C-2′), 159.3 (C-4′), and 164.6 (C-6′), and three ketone carbonyl groups at δ_C 197.9 (C-2), 208.9 (C-7′), and 211.7 (C-4). Comparison of the abovementioned spectral data with those of myrtucommulone B (phloroglucinal **13**) [20] revealed close similarity, with the exception that a 2-methylbutyl unit replaced an isobutyl at C-1 in myrtucommulone B. This structural feature was supported by a 4.35 (H-7)/1.56 (H-8)/1.50 (H_2-10a) and 1.03 (H_2-10b) and 0.74 (H_3-9)/0.90 (H_3-11) spin system identified through ^{1}H–^{1}H COSY analysis, along with key HMBC cross-peaks (Fig. 2) from δ_H 4.35 (H-7) to δ_C 103.0 (C-2′), 112.7 (C-1), 153.8 (C-2′), 159.3 (C-4′), 167.5 (C-6), and 197.9 (C-2). The H-7 was stochastically assigned as a *β* configuration, and the relative configuration for the side chain at C-7 was determined by a theoretical NMR calculation method (Fig. 3) and DP4+ probability analysis. Finally, the absolute configuration of compound **3** was established as (7*S*,8*S*) based on the ECD calculations (Fig. 4). Thus, phloroglucinol **3** was identified as a PPHTD and designated rhodotomentodimer I.

Phloroglucinols **4** and **5** were both assigned shared the molecular formula $C_{25}H_{32}O_6$, supported by HRESIMS $[M+H]^+$ peaks at *m*/*z* 429.2275 and 429.2277 (both calcd for $C_{25}H_{33}O_6$, 429.2272), respectively. Further examination of 1D NMR data (Table 3) with that of callistenone B (**14**) [20] revealed a substitution C-1′, where the isovaleryl group in **14** was replaced by a 2-methylbutanoyl moiety in both compounds. This structural change was validated by HMBC correlation between Me-9′ and C-7′ and ^{1}H–^{1}H COSY cross-peaks linking H-8′/H_2-10′ and H_3-9′/H_3-11′ (Fig. 2). The relative configurations for H-7 in compounds **4** and **5** were assigned as *α* and *β* configurations, respectively, and the relative configurations for the C-7′ side chains were determined according to further NMR calculations and DP4+ probability analysis (Fig. 3). In light of ECD calculations (Fig. 4), the absolute configuration of phloroglucinol **4** was established as (7*R*,8′*S*), and comparison of experimental ECD spectra of **5** and **4** led to the establishment of absolute configuration for **5** to be (7*S*,8′*S*). Based on spectral and computational evidence, the two structures were characterized as two PPHTDs and designated rhodotomentodimer J and rhodotomentodimer K, respectively.

Phloroglucinols **6** and **7** shared the molecular formula $C_{26}H_{34}O_6$, as indicated by their HRESIMS $[M+H]^+$ signals at *m*/*z* 443.2435 and 443.2438 (both calcd for $C_{26}H_{35}O_6$, 443.2428), respectively. Their 1D NMR spectra (Table 4) were highly similar to those of phloroglucinol **3**, suggesting structural similarity to PPHTD congeners. A distinguishing feature was the presence of a 2-methylbutyl moiety at C-1′, evidenced by disclosed by HMBC correlations of H_3-9′ with C-7′ and of OH-6′ with C-1′ as well as a COSY defined spin system of H_3-9′/H-8′/H_2-10′/H_3-11′ (Fig. 2). The relative configurations for H-7 in compounds **6** and **7** were randomly assigned as *α* and *β* configurations, respectively, and further NMR calculations and DP4+ probability analysis allowed the establishment of the relative configurations for the C-7′ side chains (Fig. 3). Owing to ECD calculations (Fig. 4), the absolute configurations of phloroglucinols **6** and **7** were established to be (7*R*,8*S*,8′*S*) and (7*S*,8*R*,8′*S*), respectively. Based on these spectroscopic and computational results, phloroglucinols **6** and **7** were identified as two two PPHTDs and designated rhodotomentodimer L and rhodotomentodimer M, respectively.

Phloroglucinol **8** was assigned the same molecular formula $C_{26}H_{34}O_6$, identical to that of **7**, as indicated

Table 3 ^{13}C (150 MHz) and ^{1}H (600 MHz) data for phloroglucinols **3**–**5** in $CDCl_3$

No	3		4		5	
	δ_C	δ_H, mult. (*J* in Hz)	δ_C	δ_H, mult. (*J* in Hz)	δ_C	δ_H, mult. (*J* in Hz)
1	112.7, s		112.1, s		112.1, s	
2	197.9, s		198.4, s		198.7, s	
3	56.2, s		56.2, s		56.2, s	
4	211.7, s		211.8, s		211.8, s	
5	47.2, s		47.3, s		47.3, s	
6	167.5, s		168.0, s		168.1, s	
7	30.9, d	4.35, d (3.0)	31.5, d	4.35, d (3.5)	31.5, d	4.31, d (3.6)
8	42.1, d	1.56, m	34.8, d	1.91, m	34.8, d	1.92, m
9	14.9, q	0.74, d (6.8)	18.7, q	0.83, d (6.9)	18.6, q	0.79, d (6.9)
10	26.1, t	a 1.50, m	18.8, q	0.79, d (6.9)	18.8, q	0.84, d (6.9)
		b 1.03, m				
11	12.3, q	0.90, t (7.3)	24.2, q	1.39, s	24.0, q	1.38, s
12	24.3, q	1.39, s	25.1, q	1.45, s	25.1, q	1.45, s
13	24.5, q	1.43, s	24.8, q	1.45, s	24.9, q	1.41, s
14	24.9, q	1.42, s	25.0, q	1.63, s	25.1, q	1.63, s
15	25.1, q	1.61, s				
1′	104.0, s		104.2, s		105.1, s	
2′	153.8, s		153.5, s		153.6, s	
3′	103.0, s		103.6, s		103.7, s	
4′	159.3, s		159.3, s		159.5, s	
5′	100.6, d	6.26, s	100.7, s	6.29, s	100.5, d	6.27, s
6′	164.6, s		165.0, s		164.1, s	
7′	208.9, s		208.7, s		209.2, s	
8′	39.7, d	3.90, sept. (6.8)	46.9, d	3.76, sext. (7.0)	45.5, d	3.89, sext. (6.7)
9′	17.7, q	1.25, d (6.7)	18.8, q	1.22, d (7.2)	15.6, q	1.26, d (6.6)
10′	20.8, q	1.24, d (7.3)	24.7, t	a 1.96, m	28.6, t	a 1.75, m
				b 1.50, m		b 1.57, m
11′			12.1, q	0.98, t (7.4)	11.2, q	0.85, t (7.4)
OH-6′		13.30, s		13.54, s		13.13, s

by its HRESIMS peak at *m*/*z* 443.2431 $[M+H]^+$ (calcd for $C_{26}H_{35}O_6$, 443.2428). Analysis of the ^{13}C NMR spectrum (Table 4), supported by HSQC and DEPT data, revealed 26 carbon resonances, including three keto carbonyls, an aromatic ring, four quaternary carbons (two olefinic ones), three methine groups, two methene groups, and eight methyl groups. Comparison of phloroglucinol **8** and rhodotomentodimer D (**10**) [13] indicated the replacement of the isopentyl side chain at C-1 by a 2-methylbutyl group. This substitution was corroborated by a ^{1}H–^{1}H COSY spin system (Fig. 2) of δ_H 4.32 (H-7)/1.60 (H-8)/1.45 (H_2-10a) and 1.01 (H_2-10b) and 0.71 (H_3-9)/0.89 (H_3-11) and HMBC correlations of δ_H 4.32 (H-7) with δ_C 104.4 (C-3′), 112.6 (C-1), 156.6 (C-4′), 162.3 (C-2′), 167.6 (C-6), and 197.6 (C-2). The relative configuration of H-7 in compound **8** was stochastically assigned to be *β* orientated, the *β* configuration for the C-8 and C-8′ ethyl groups were determined by theoretical NMR calculations and DP4+ probability analysis (Fig. 3). Subsequent ECD calculations (Fig. 4) permitted the assignment of the absolute configuration for phloroglucinol **8** to be (7*S*,8*R*,8′*S*). Hence, phloroglucinol **8** was identified as a PPHTD and named rhodotomentodimer N.

Given that rhodotomentodimer D (**10**) [16], a structurally related analogue, exhibited inhibitory activity against human acetylcholinesterase (*h*AChE), further screening was conducted to assess this activity among related compounds (Table 5). All PPHTDs (**3**–**14**) demonstrated significant *h*AChE inhibition, with IC_{50} values between 1.04 and 3.35 μM. In contrast, phloroglucinols **1** and **2** were inactive, with IC_{50} values exceeding 40.0 μM.

To gain insights into the binding modes of excellent *h*AChE inhibitor **13**, molecular docking was carried out using the crystal structure of recombinant *h*AChE

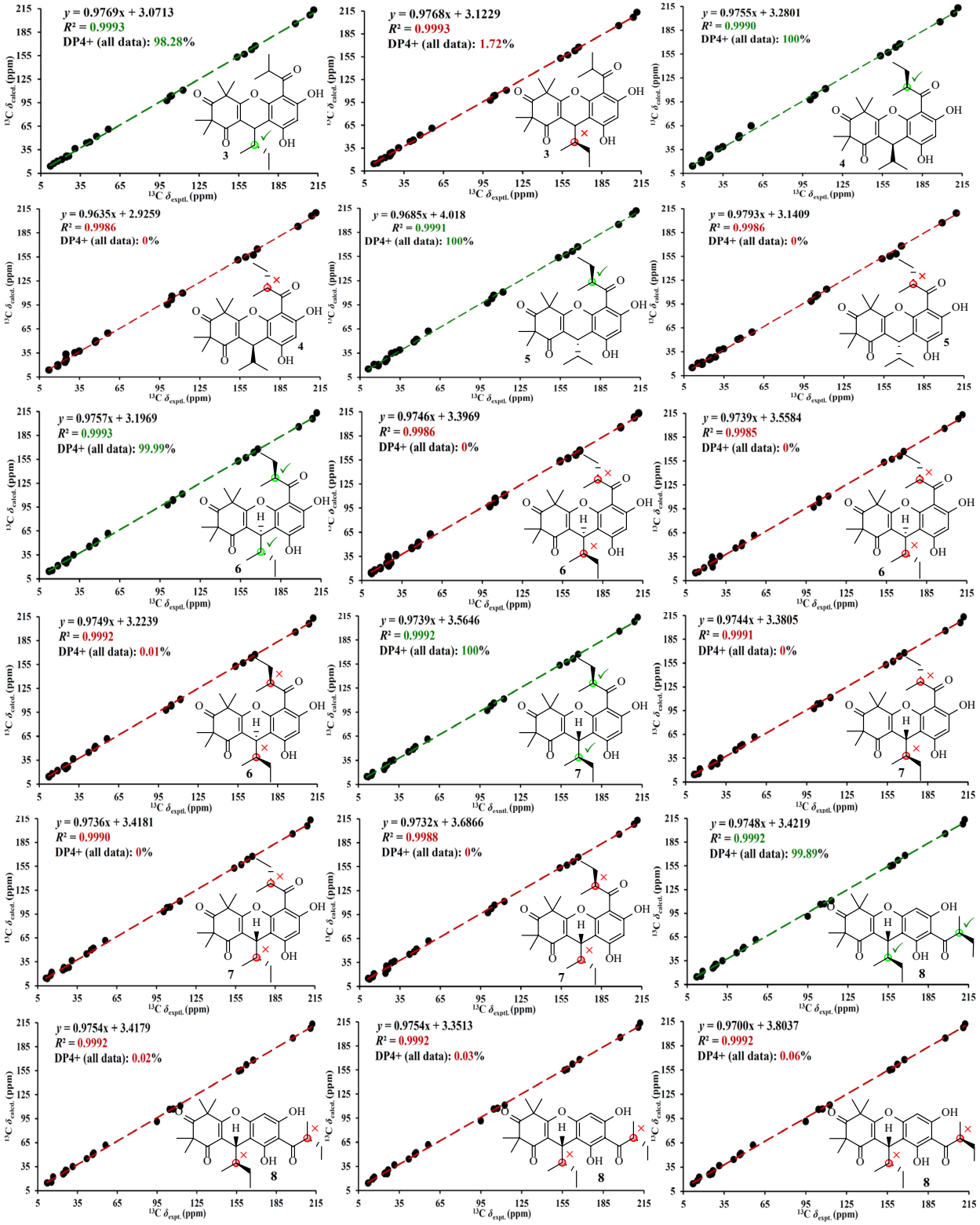

Fig. 3 NMR calculations and DP4+ analyses for phloroglucinols **3**–**8**

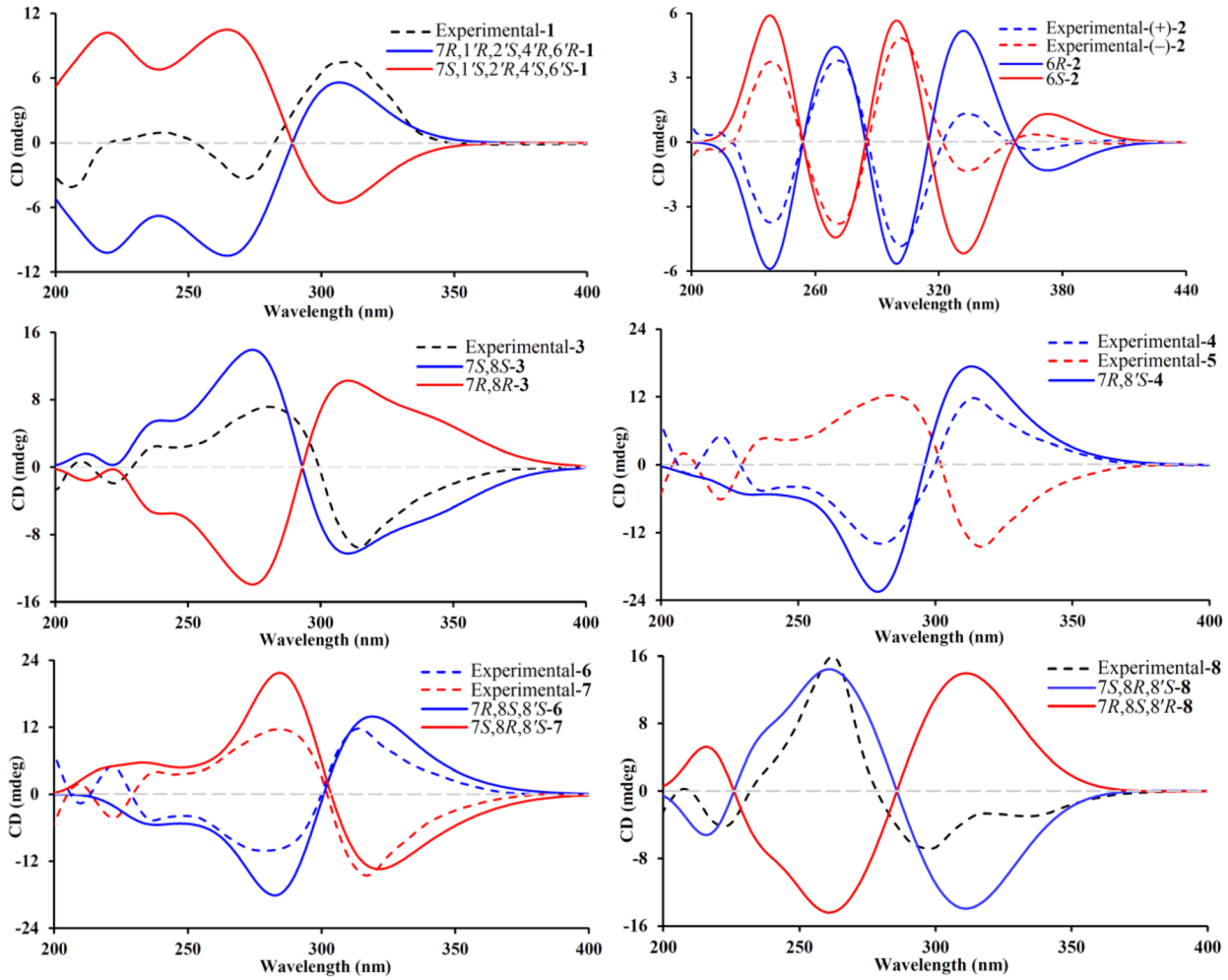

Fig. 4 Calculated and experimental ECD spectra of phloroglucinols **1**–**8**

complex with (−)-galantamine (PDB code: 4EY6, 2.40 Å resolution) [22]. The docking results indicated that phloroglucinol **13** fits well within the active site pocket of *h*AChE (Fig. 5). Apart from a π–σ stacking interaction with Tyr337 (3.61 Å), five hydrogen bonds were observed between phloroglucinol **13** and the residues Gly120 (2.46 Å), Tyr133 (1.67 Å), Glu202 (2.13 Å), Ser203 (2.24 Å), and His447 (2.39 Å).

In light of well-documented antibacterial activity of rhodomyrtone (**12**) [23–26], other phloroglucinol compounds were also assessed for their inhibitory effects on vancomycin-resistant *Enterococci* (VRE). Phloroglucinols **11** and **12** exhibited strong activity (MIC = 1 μg/mL), outperforming ampicillin (AMP, MIC = 2 μg/mL). Similarly, phloroglucinols **8**–**10** showed comparable potency (MIC = 2 μg/mL). In contrast, phloroglucinols **1**–**7**, **13**, and **14** were inactive (MIC > 32 μg/mL). These findings suggested that the different connection patterns of PPHTDs can significantly affect their antibacterial properties, thereby offering valuable insights for the design and synthesis of novel antibacterial agents.

3 Conclusions

A total of 14 diverse phloroglucinol derivatives (**1**–**14**), including eight newly identified isolates (**1**–**8**), were obtained from *R. tomentosa* fruits. The absolute configurations of the side chains in phloroglucinols **3**–**8** were unambiguously determined through a combination of ECD computations, NMR calculations, and DP4+ probability assessments. In addition, the previously reported phloroglucinol dimers (**9**–**14**) were obtained from *R. tomentosa* fruits for the first time, and several of them represent characteristic and major bioactive constituents of both *R. tomentosa* and *Myrtus communis*. Notably, many of the isolated compounds demonstrated

Table 4 ^{13}C (150 MHz) and ^{1}H (600 MHz) data for **6**–**8** in $CDCl_3$

No	6		7		8	
	δ_C	δ_H, mult. (*J* in Hz)	δ_C	δ_H, mult. (*J* in Hz)	δ_C	δ_H, mult. (*J* in Hz)
1	111.6, s		112.7, s		112.6, s	
2	198.4, s		198.1, s		197.6, s	
3	56.2, s		56.2, s		56.2, s	
4	211.8, s		211.7, s		212.2, s	
5	47.4, s		47.2, s		47.2, s	
6	167.9, s		167.7, s		167.6, s	
7	30.5, d	4.42, d (3.2)	30.9, d	4.37, d (2.8)	31.4, d	4.32, d (3.0)
8	42.3, d	1.62, m	42.1, d	1.57, m	41.9, d	1.60, m
9	14.6, q	0.77, d (6.9)	14.7, q	0.75, d (6.8)	15.3, q	0.71, d (6.9)
10	26.6, t	a 1.43, m	26.1, q	a 1.51, m	26.3, t	a 1.45, m
		b 0.92, m		b 1.03, m		b 1.01, m
11	12.4, q	0.92, t (7.3)	12.3, q	0.90 t (7.3)	12.0, q	0.89 t (7.3)
12	25.1, q	1.39, s	24.2, q	1.39, s	24.1, q	1.36, s
13	25.4, q	1.45, s	24.9, q	1.44, s	24.7, q	1.41, s
14	23.7, q	1.44, s	24.6, q	1.41, s	24.6, q	1.41, s
15	25.0, q	1.63, s	25.1, q	1.62, s	25.1, q	1.57, s
1′	104.1, s		105.3, s		107.3, s	
2′	153.2, s		154.0, s		162.3, s	
3′	104.7, s		103.1, s		104.4, s	
4′	159.0, s		159.3, s		156.6, s	
5′	100.7, d	6.27, s	100.4, d	6.26, s	94.9, d	6.10, s
6′	164.9, s		164.0, s		158.5, s	
7′	208.7, s		209.3, s		210.8, s	
8′	46.8, d	3.76, sext. (6.9)	45.5, d	3.88, sext. (6.6)	46.5, d	3.74, sext. (6.7)
9′	18.8, q	1.23, d (7.1)	15.6, q	1.26, d (6.6)	16.6, q	1.18, d (6.8)
10′	24.8, t	a 1.96, m	28.6, t	a 1.75, m	26.8, t	a 1.87, m
		b 1.50, m		b 1.56, m		b 1.43, m
11′	12.1, q	0.98, t (7.4)	11.2, q	0.85, t (7.5)	12.4, q	0.94, t (7.4)
OH-2′						7.51, s
OH-6′		13.54, s		13.12, s		12.30, s

Table 5 *h*AChE inhibitory activities of phloroglucinols **1**–**9** and **11**–**14**

Compounds	$IC_{50} \pm SD$ (μM)	Compounds	$IC_{50} \pm SD$ (μM)
1	> 40.0	**8**	3.35 ± 0.41
2	> 40.0	**9**	2.86 ± 0.30
3	2.89 ± 0.30	**11**	1.36 ± 0.16
4	2.39 ± 0.25	**12**	1.52 ± 0.14
5	2.46 ± 0.33	**13**	1.04 ± 0.03
6	2.62 ± 0.21	**14**	1.23 ± 0.11
7	2.41 ± 0.22	Galanthamine	1.06 ± 0.05

potent *h*AChE inhibitory activities, highlighting their potential as lead candidates for the treatment of neurological disorders, including Alzheimer's disease [27]. Furthermore, several isolates exhibited significant anti-VRE effects, underscoring the therapeutic promise of *R. tomentosa* fruits for combating drug-resistant bacterial infections [28, 29]. Given the limited prior knowledge of the phloroglucinol constituents of *R. tomentosa* fruits, the present findings significantly expand current understanding and provide a scientific basis for the future development of nutraceutical and medicinal food products.

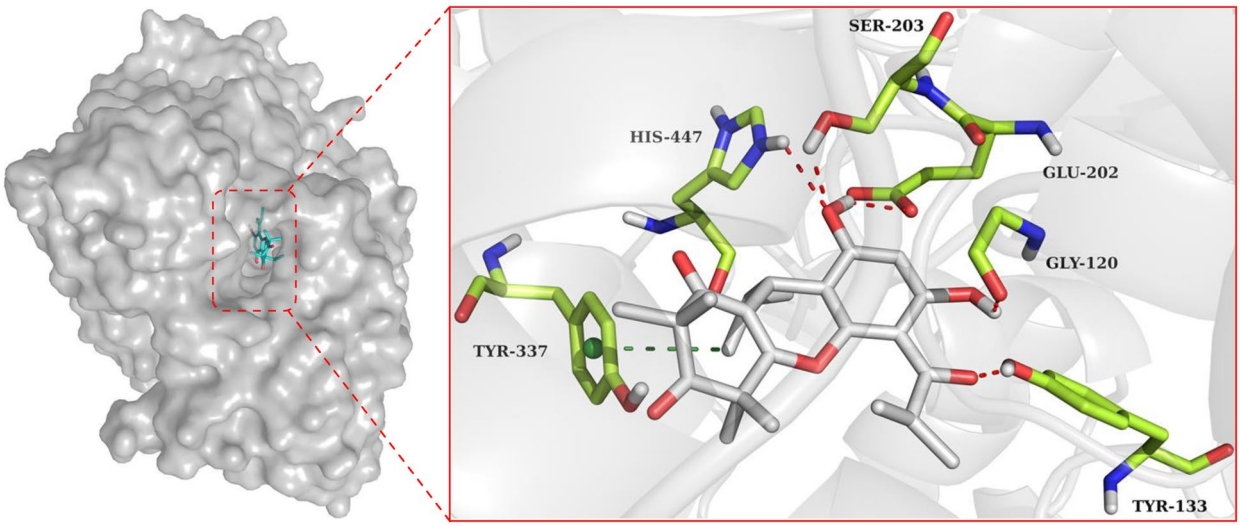

Fig. 5 Molecular docking of phloroglucinol **13** with *h*AChE

4 Experimental procedures

4.1 General experimental procedures

The experimental procedures followed those previously reported in our recent publication [30].

4.2 Plant material

The mature fruits of *R. tomentosa* were collected in Wanning, Hainan province, China, in September 2023. The plant material was authenticated by Xin-Quan Yang (Hainan Branch Institute of Medicinal Plant Development, Chinese Academy of Medical Sciences). A voucher specimen (KIB-Q-202301) has been deposited at the State Key Laboratory of Phytochemistry and Natural Medicines, Kunming Institute of Botany, Chinese Academy of Sciences.

4.3 Extraction and isolation

The air-dried and powdered fruits of *R. tomentosa* (19.5 kg) were extracted thrice with ethanol at room temperature (48 h). The ethanol extracts were concentrated under reduced pressure, to afford a crude residue (1.56 kg), which was partitioned with petroleum ether (PE) and ethyl acetate (EtOAc), yielding PE (331 g) and EtOAc-soluble (282 g) fractions. To eliminate lipoid components, the PE extract was further partitioned with MeOH–H_2O (8:2, *v*/*v*), yielding a phloroglucinol enriched moiety (58.0 g). This enriched extract was subjected to silica gel column chromatography with a PE–EtOAc (100:1 → 1:1, *v*/*v*) gradient, yielding seven main fractions (Fr. A–Fr. G). Fr. A (28.6 g) was further separated on silica gel (PE–EtOAc, 100:0 → 0:100, *v*/*v*), producing three subfractions (Fr. A_1–Fr. A_3). Fr. A_1 (6.7 g) was purified by an RP-C18 column (MeOH–H_2O, 70:30 → 100:0, *v*/*v*), producing six subfractions (Fr. $A_{1.1}$–Fr. $A_{1.6}$). Compound **12** (4 mg) was obtained from Fr. $A_{1.1}$ via recrystallization d (Acetone–MeOH, 10:1, *v*/*v*), while **10** (2.8 mg, t_R = 36 min) was isolated from Fr. $A_{1.2}$ (0.05 g) by semi-preparative HPLC (MeOH–H_2O, 83:17, *v*/*v*). Fr. B (13 g) was separated by silica gel chromatography (PE–EtOAc, 15:1 → 0:16, *v*/*v*), resulting in seven subfractions (Fr. B_1–Fr. B_7). Fr. B_1 (0.3 g) was further purified via semi-preparative HPLC (MeCN–H_2O, 52:48, *v*/*v*) to afford compounds **9** (3.1 mg, t_R = 33 min) and **13** (10.5 mg, t_R = 49 min). Fr. C (12 g) underwent RP-C_{18} chromatography (MeOH–H_2O, 70:30 → 100:0, *v*/*v*), yielding five fractions (Fr. C_1–Fr. C_5). Fr. C_2 (0.18 g) was further purified by a semi-preparative HPLC (MeCN–H_2O, 80:20, *v*/*v*), affording compounds **3** (1.4 mg, t_R = 18 min) and **5** (3.0 mg, t_R = 15 min). Fr. D (16 g) was fractionated by an RP-C_{18} column (MeOH–H_2O, 75:25 → 100:0, *v*/*v*), resulting in six subfractions (Fr. D_1–Fr. D_6). Fr. D_2 (0.92 g) afforded compounds **1** (2.0 mg, t_R = 35 min) and **8** (2.2 mg, t_R = 40 min) by semi-preparative HPLC (MeCN–H_2O, 73:27, *v*/*v*). Likewise, compound **2** (3.2 mg, t_R = 42 min) was isolated from Fr. D_4 (0.65 g) by a semi-prep. HPLC (MeCN–H_2O, 65:35, *v*/*v*). Fr. E (2 g) was separated on Sephadex LH-20 ($CHCl_3$–MeOH, 1:1, *v*/*v*), giving three fractions (Fr. E_1–Fr. E_3). Fr. E_1 (0.39 g) was subjected to semi-preparative HPLC (MeCN–H_2O, 60:40, *v*/*v*), yielding compounds **4** (3 mg, t_R = 32 min), **11** (7.2 mg, t_R = 40 min), **6** (2.6 mg, t_R = 44 min), **7** (3 mg, t_R = 42 min), and **14** (7.0 mg, t_R = 37 min). Chiral separation of compound **2** was achieved using a Daicel CHIRALPAK IC column (*n*-hexane–isopropanol, 95:5 → 85:15, *v*/*v*), furnishing enantiomers (+)-**2** (1.0 mg, t_R = 12 min) and (−)-**2** (1.0 mg, t_R = 13 min).

Rhodotomentodione F (**1**): Colorless gum; [α] + 28.1 (*c* 0.1, MeOH); UV (MeOH) λ_{max} (log ε) 268 (3.68) nm; ECD (MeOH) λ_{max} ($\Delta\varepsilon$) 205(−5.36), 241 (+1.25), 271 (−4.41), 311 (+9.76) nm; ^{1}H (600 MHz, $CDCl_3$) and ^{13}C (150 MHz, $CDCl_3$) NMR data, see Table 1; (+)-HRESIMS *m*/*z* 387.2904 $[M+H]^+$ (calcd for $C_{25}H_{38}O_3$, 387.2894).

Rhodotomentodimer H (**2**): Colorless gum; [α] + 49.0 (*c* 0.10, MeOH) for (+)-**2**; [α] −49.0 (*c* 0.10, MeOH) for (−)-**2**; UV (MeOH) λ_{max} (log ε) 217 (2.68), 272 (2.52) nm; ECD (MeOH) λ_{max} ($\Delta\varepsilon$) 239 (−4.49), 271 (+4.56), 301 (−5.83), 333 (+1.61) nm for (+)-**2**; ECD (MeOH) λ_{max} ($\Delta\varepsilon$) 239 (+4.49), 271 (−4.56), 301 (+5.83), 333 (−1.61) nm for (−)-**2**; ^{1}H (600 MHz, $CDCl_3$) and ^{13}C (150 MHz, $CDCl_3$) NMR data, see Table 2; (+)-HRESIMS *m*/*z* 375.1802 $[M+H]^+$ (calcd for $C_{21}H_{27}O_6$, 375.1802).

Rhodotomentodimer I (**3**): Colorless gum; [α] −85.4 (*c* 0.10, MeOH); UV (MeOH) λ_{max} (log ε) 203 (4.08), 216 (4.06), 295 (3.87) nm; ECD (MeOH) λ_{max} ($\Delta\varepsilon$) 209 (+0.34), 222 (−1.01), 238 (+1.26), 280 (+3.70), 314 (−4.94) nm; ^{1}H (600 MHz, $CDCl_3$) and ^{13}C (150 MHz, $CDCl_3$) NMR data, see Table 3; (+)-HRESIMS *m*/*z* 429.2279 $[M+H]^+$ (calcd for $C_{25}H_{33}O_6$, 429.2272).

Rhodotomentodimer J (**4**): Colorless gum; [α] + 149.4 (*c* 0.10, MeOH); UV (MeOH) λ_{max} (log ε) 203 (4.27), 217 (4.26), 295 (4.10) nm; ECD (MeOH) λ_{max} ($\Delta\varepsilon$) 209 (−1.19), 221 (+3.65), 237 (−3.38), 280 (−10.08), 313 (+8.51) nm; ^{1}H (600 MHz, $CDCl_3$) and ^{13}C (150 MHz, $CDCl_3$) NMR data, see Table 3; (+)-HRESIMS *m*/*z* 429.2275 $[M+H]^+$ (calcd for $C_{25}H_{33}O_6$, 429.2272).

Rhodotomentodimer K (**5**): Colorless gum; [α] −186.6 (*c* 0.10, MeOH); UV (MeOH) λ_{max} (log ε) 203 (4.26), 216 (4.27), 294 (4.16) nm; ECD (MeOH) λ_{max} ($\Delta\varepsilon$) 208 (+1.49), 221 (−4.50), 238 (−3.40), 283 (+8.83), 316 (−10.50) nm; ^{1}H (600 MHz, $CDCl_3$) and ^{13}C (150 MHz, $CDCl_3$) NMR data, see Table 3; (+)-HRESIMS *m*/*z* 429.2277 $[M+H]^+$ (calcd for $C_{25}H_{33}O_6$, 429.2272).

Rhodotomentodimer L (**6**): Colorless gum; [α] + 83.7 (*c* 0.10, MeOH); UV (MeOH) λ_{max} (log ε) 203 (4.10), 217 (4.10), 295 (3.98) nm; ECD (MeOH) λ_{max} ($\Delta\varepsilon$) 209 (−0.79), 221 (+2.42), 237 (−2.24), 278 (−4.85), 313 (+5.65) nm; ^{1}H (600 MHz, $CDCl_3$) and ^{13}C (150 MHz, $CDCl_3$) NMR data, see Table 4; (+)-HRESIMS *m*/*z* 443.2435 $[M+H]^+$ (calcd for $C_{26}H_{35}O_6$, 443.2428).

Rhodotomentodimer M (**7**): Colorless gum; [α] −85.4 (*c* 0.10, MeOH); UV (MeOH) λ_{max} (log ε) 205 (4.25), 218 (4.27), 297 (4.15) nm; ECD (MeOH) λ_{max} ($\Delta\varepsilon$) 209 (+1.22), 222 (−2.88), 238 (+2.69), 283 (+7.78), 316 (−9.79) nm; ^{1}H (600 MHz, $CDCl_3$) and ^{13}C (150 MHz, $CDCl_3$) NMR data, see Table 4; (+)-HRESIMS *m*/*z* 443.2438 $[M+H]^+$ (calcd for $C_{26}H_{35}O_6$, 443.2428).

Rhodotomentodimer N (**8**): Colorless gum; [α] −60.2 (*c* 0.10, MeOH); UV (MeOH) λ_{max} (log ε) 202 (4.02), 225 (3.99), 263 (3.73), 301 (3.88) nm; ECD (MeOH) λ_{max} ($\Delta\varepsilon$) 207 (+0.20), 222 (−2.94), 262 (+11.13), 297 (−4.81) nm; ^{1}H (600 MHz, $CDCl_3$) and ^{13}C (150 MHz, $CDCl_3$) NMR data, see Table 4; (+)-HRESIMS *m*/*z* 443.2431 $[M+H]^+$ (calcd for $C_{26}H_{35}O_6$, 443.2428).

4.4 ECD and NMR calculations

ECD and NMR computations were carried out based on previously reported methods using the Gaussian 16 software package [14]. Three-dimensional molecular structures were constructed based on ROESY spectra (for compound **1**) or randomly generated (for compounds **2**–**8**), followed by conformational analysis using CONFLEX with the MMFF94S force field. ECD and NMR chemical shift calculations were conducted at the B3LYP/6–311++G(2d,p) and mPW1PW91/6–31+G(d,p) levels, respectively. The DP4+ probability analyses were accomplished utilizing a published computational template [31].

4.5 Human AChE inhibitory assay

*h*AChE inhibition assays were performed according to a reported protocol, with galantamine as the positive control [32]. All assays were performed in triplicate. Compounds with IC_{50} values exceeding 40 μM were considered inactive.

4.6 Anti-VRE assay

As described in earlier studies, the antibacterial activities against vancomycin-resistant *Enterococci* (VRE) were achieved by a standard broth microdilution method in 96-well plates [33]. Ampicillin (AMP) was a positive control, and all tests were performed three times.

4.7 Molecular docking

Molecular docking simulations were performed utilizing the AutoDock software suit [34], following established protocols. The docking complexes of phloroglucinol **13** with *h*AChE (PDB ID: 4EY6) were generated, and the resulting binding poses were visualized utilizing the PyMOL Molecular Graphics System.

Supplementary Information

The online version contains supplementary material available at https://doi.org/10.1007/s13659-025-00557-0.

Supplementary material 1.

Acknowledgements

This study was financially supported by the National Natural Science Foundation of China (32270425 and 31970377), the Yunnan Fundamental Research Projects (202501AS070093, 202201AT070181, and 202401AT070191), the Top Young Talent of Ten Thousand Talents Program of Yunnan Province

(YNWR-QNBJ-2020-253), the Reserve Talents of Young and Middle-Aged Academic and Technical Leaders of Yunnan Province (202105AC160023), and CAS Light of West China Program. We are grateful to Analysis and Testing Centre (Kunming Institute of Botany, Chinese Academy of Sciences) for NMR, HRESIMS, CD, and bioactive measurement.

Author contributions
Ling-Yun Chen carried out the experiments and prepared the original draft; Mu-Yuan Yu participated in the main experiments and revised the manuscript; E-E Luo and Wen-Ying Zong performed the ECD calculations; Shu-Mei Lei and Yu Pan performed the NMR calculations; Ai-Chun Lu and Cheng-Qin Liang revised the manuscript; Xu-Jie Qin conceived and supervised the study, revised the manuscript, and secured project funding. All authors reviewed and approved the final version of the manuscript.

Data availability
The datasets used or analyzed during the current study are available from the corresponding author on reasonable request.

Declarations

Competing interests
The authors declare that they have no known competing financial interests or personal relationships that could have appeared to influence the work reported in this paper.

Author details
[1]College of Pharmacy, Guilin Medical University, Guilin 541199, People's Republic of China. [2]State Key Laboratory of Phytochemistry and Natural Medicines, Kunming Institute of Botany, Chinese Academy of Sciences, Kunming 650201, People's Republic of China. [3]University of Chinese Academy of Sciences, Beijing 100049, People's Republic of China.

Received: 28 May 2025 Accepted: 4 October 2025
Published online: 08 January 2026

References

1. Celaj O, Duarán AG, Cennamo P, Scognamiglio M, Fiorentino A, Esposito A, et al. Phloroglucinols from Myrtaceae: attractive targets for structural characterization, biological properties and synthetic procedures. Phytochem Rev. 2021;20(1):259–99.
2. Saising J, Ongsakul M, Voravuthikunchai SP. *Rhodomyrtus tomentosa* (Aiton) Hassk. ethanol extract and rhodomyrtone: a potential strategy for the treatment of biofilm-forming staphylococci. J Med Microbiol. 2011;60(12):1793–800.
3. Hu X, Chen Y, Dai J, Yao L, Wang L. *Rhodomyrtus tomentosa* fruits in two ripening stages: chemical compositions, antioxidant capacity and digestive enzymes inhibitory activity. Antioxidants. 2022;11(7):1390.
4. Cui C, Zhang S, You L, Ren J, Luo W, Chen W, et al. Antioxidant capacity of anthocyanins from *Rhodomyrtus tomentosa* (Ait.) and identification of the major anthocyanins. Food Chem. 2013;139(1–4):1–8.
5. Lai TNH, André C, Rogez H, Mignolet E, Nguyen TBT, Larondelle Y. Nutritional composition and antioxidant properties of the sim fruit (*Rhodomyrtus tomentosa*). Food Chem. 2015;168:410–6.
6. Wu P, Ma G, Li N, Deng Q, Yin Y, Huang R. Investigation of in vitro and in vivo antioxidant activities of flavonoids rich extract from the berries of *Rhodomyrtus tomentosa* (Ait.) Hassk. Food Chem. 2015;173:194–202.
7. Shiratake S, Nakahara T, Iwahashi H, Onodera T, Mizushina Y. Rose myrtle (*Rhodomyrtus tomentosa*) extract and its component, piceatannol, enhance the activity of DNA polymerase and suppress the inflammatory response elicited by UVB-induced DNA damage in skin cells. Mol Med Rep. 2015;12(4):5857–64.
8. Wang R, Yao L, Lin X, Hu X, Wang L. Exploring the potential mechanism of *Rhodomyrtus tomentosa* (Ait.) Hassk fruit phenolic rich extract on ameliorating nonalcoholic fatty liver disease by integration of transcriptomics and metabolomics profiling. Food Res Int. 2022;151:110824.
9. Wang R, Yao L, Meng T, Li C, Wang L. *Rhodomyrtus tomentosa* (Ait.) Hassk fruit phenolic-rich extract mitigates intestinal barrier dysfunction and inflammation in mice. Food Chem. 2022;393:133438.
10. Lai TNH, Herent MF, Leclercq JQ, Nguyen TBT, Rogez H, Larondelle Y, et al. Piceatannol, a potent bioactive stilbene, as major phenolic component in *Rhodomyrtus tomentosa*. Food Chem. 2013;138(2–3):1421–30.
11. Zhuang L, Chen LF, Zhang YB, Liu Z, Xiao XH, Tang W, et al. Watsonianone a from *Rhodomyrtus tomentosa* fruit attenuates respiratory-syncytial-virus-induced inflammation in vitro. J Agric Food Chem. 2017;65(17):3481–9.
12. Chen LY, Luo EE, Pan Y, Liang CQ, Yu MY, Qin XJ. Acetylcholinesterase inhibitory phloroglucinols from tropic *Rhodomyrtus tomentosa*. Phytochemistry. 2024;228:114254.
13. Luo EE, Liu SN, Wang ZJ, Chen LY, Liang CQ, Yu MY, et al. Oligomeric phloroglucinols with *h*AChE inhibitory and antibacterial activities from tropic *Rhodomyrtus tomentosa*. Bioorg Chem. 2023;141:106836.
14. Qin XJ, Liu H, Li PP, Ni W, He L, Khan A, et al. Polymethylated acylphloroglucinols from *Rhodomyrtus tomentosa* exert acetylcholinesterase inhibitory effects. Bioorg Chem. 2021;107:104519.
15. Qin XJ, Rauwolf TJ, Li PP, Liu H, McNeely J, Hua Y, et al. Isolation and synthesis of novel meroterpenoids from *Rhodomyrtus tomentosa*: Investigation of a reactive enetrione intermediate. Angew Chem Int Ed. 2019;58(13):4291–6.
16. Yu MY, Liu SN, Luo EE, Jin Q, Liu H, Liu HY, et al. Phloroglucinols with *h*AChE and *α*-glucosidase inhibitory activities from the leaves of tropic *Rhodomyrtus tomentosa*. Phytochemistry. 2022;203:113394.
17. Kaneshima T, Myoda T, Toeda K, Fujimori T, Nishizawa M. Antimicrobial constituents of peel and seeds of camu-camu (*Myrciaria dubia*). Biosci Biotechnol Biochem. 2017;81(8):1461–5.
18. Tanaka N, Jia Y, Niwa K, Imabayashi K, Tatano Y, Yagi H, et al. Phloroglucinol derivatives and a chromone glucoside from the leaves of *Myrtus communis*. Tetrahedron. 2018;74(1):17–123.
19. Salni D, Sargent MV, Skelton BW, Soediro I, Sutisna M, White AH, et al. Rhodomyrtone, an antibiotic from *Rhodomyrtus tomentosa*. Aust J Chem. 2002;55(3):229–32.
20. Charpentier M, Hans M, Jauch J. Enantioselective synthesis of myrtucommulone A. Eur J Org Chem. 2013;2013(19):4078–84.
21. Rattanaburi S, Mahabusarakam W, Phongpaichit S, Carroll AR. Acylphloroglucinols from *Callistemon lanceolatus* DC. Tetrahedron. 2013;69(30):6070–5.
22. Cheung J, Rudolph MJ, Burshteyn F, Cassidy MS, Gary EN, Love J, et al. Structures of human acetylcholinesterase in complex with pharmacologically important ligands. J Med Chem. 2012;55(22):10282–6.
23. Leejae S, Taylor PW, Voravuthikunchai P. Antibacterial mechanisms of rhodomyrtone against important hospital-acquired antibiotic-resistant pathogenic bacteria. J Med Microbiol. 2013;62(1):78–85.
24. Limsuwan S, Hesseling-Meinders A, Voravuthikunchai SP, Dijl JM, Kayser O. Potential antibiotic and anti-infective effects of rhodomyrtone from *Rhodomyrtus tomentosa* (Aiton) Hassk. on *Streptococcus pyogenes* as revealed by proteomics. Phytomedicine. 2011;18(11):934–40.
25. Rani R, Righetto GM, Schäfer AB, Wenzel M. The diverse activities and mechanisms of the acylphloroglucinol antibiotic rhodomyrtone: antibacterial activity and beyond. Antibiotics. 2024;13(10):936.
26. Srisuwan S, Mackin KE, Hocking D, Lyras D, Bennett-Wood V, Voravuthikunchai SP, et al. Antibacterial activity of rhodomyrtone on *Clostridium difficile* vegetative cells and spores in vitro. Int J Antimicrob Agents. 2018;52(5):724–9.
27. Singh M, Kaur M, Kukreja H, Chugh R, Silakari O, Singh D. Acetylcholinesterase inhibitors as Alzheimer therapy: from nerve toxins to neuroprotection. Eur J Med Chem. 2013;70:165–88.
28. Kumar G, Engle K. Natural products acting against *S. aureus* through membrane and cell wall disruption. Nat Prod Rep. 2023;40(10):1608–46.
29. Wang ZJ, Zhu YY, Bai LY, Tang DM, Zhou ZS, Wei MZ, et al. A new therapeutic strategy for infectious diseases against intracellular multidrug-resistant bacteria. J Control Release. 2024;375:467–77.
30. Luo EE, Yang WF, Wang ZJ, Chen LY, Yu MY, Luo XD, et al. Phytocannabinoid-like meroterpenoids from twigs and leaves of *Rhododendron spinuliferum*. Phytochemistry. 2024;228:114241.
31. Grimblat N, Zanardi MM, Sarotti AM. Beyond DP4: an improved probability for the stereochemical assignment of isomeric compounds

using quantum chemical calculations of NMR shifts. J Org Chem. 2015;80:12526–34.
32. Liu H, He XZ, Feng MY, Zeng Y, Rauwolf TJ, Shao LD, et al. Acylphloroglucinols with acetylcholinesterase inhibitory effects from the fruits of *Eucalyptus robusta*. Bioorg Chem. 2020;103:1104127.
33. Shi YZ, Wang ZJ, Shi N, Bai LY, Jiang YM, Jiang L, et al. Anti-MRSA mechanism of spirostane saponin in Rohdea pachynema F.T. Wang & tang. J Ethnopharmacol. 2024;331:118327.
34. Yu MY, Liu SN, Liu H, Meng QH, Qin XJ, Liu HY. Acylphloroglucinol trimers from *Callistemon salignus* seeds: isolation, configurational assignment, *h*AChE inhibitory effects, and molecular docking studies. Bioorg Chem. 2021;117:105404.

Publisher's Note